I&EC research
Industrial & Engineering Chemistry Research

Article

Cite This: Ind. Eng. Chem. Res. 2018, 57, 11141−11153

pubs.acs.org/IECR

Evaluating Regeneration Options of Solid Amine Sorbent for CO_2 Removal

Martin J. Bos, Vincent Kroeze, Stevia Sutanto, and Derk W. F. Brilman*

Sustainable Process Technology, Faculty of Science and Technology, University of Twente, PO Box 217, 7500 AE Enschede, The Netherlands

ABSTRACT: Biogas is one of the most popular alternative energy resources to replace fossil fuels. The product of anaerobic fermentation in a digester contains several impurities such as H_2S and especially CO_2 that needs to be removed in order to upgrade the gas quality. Supported amine sorbents (SAS) might provide an attractive option to remove these impurities. However, little is known about the regeneration of the sorbent. This study evaluates experimentally and by modeling the options for regeneration of the SAS. Theoretically, pressure swing adsorption without purge flow is the most energy efficient method (1.7 MJ/kg CO_2). It was found that when using a purge flow the desorption rate is strongly influenced by the equilibrium between the gas and adsorbed phase. With elevated temperature (>80 °C) both the working capacity and the productivity increase significantly. Finally, an energy evaluation for a typical biogas case study is carried out, showing the trade-offs between power consumption, heat demand, and sorbent inventory. Interestingly, at the expense of a somewhat higher power consumption, the use of inexpensive air as purge gas at 60 °C could be an attractive option, but case-specific costs are needed to identify the economic optimum.

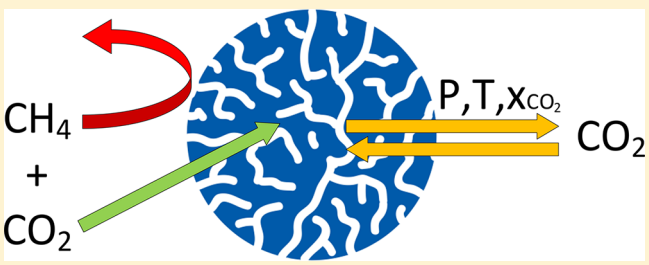

1. INTRODUCTION

Biogas is a renewable alternative energy source, which is formed via anaerobic fermentation of bio waste. It can be used directly as a fuel or as a raw material of synthesis gas, with CH_4 and CO_2 as main constituents and some other undesirable contaminants. Depending on the source of biomass, the presence and the quantity of the contaminants may fluctuate.[1] Before biogas can be utilized, the sour gas compounds (CO_2, and H_2S) and H_2O should be removed from the gas stream to prevent corrosion and to increase the heating value of the gas. The most common technology for removing these components are absorption using aqueous solvents and membrane separation.[2] The first technique requires a significant amount of energy for the recovery of the solvent, and the second method requires high capital costs and excessive maintenance.[2]

In this study, adsorption using the supported amine sorbent (SAS) Lewatit VP OC 1065 has been evaluated to upgrade methane-rich biogas to pipeline specification, especially for CO_2 removal. Methane and other components of biogas are known to be inert.[3,4] Additionally, H_2S and H_2O do adsorb but do not influence CO_2 capacity in a negative way.[4,5] Fixed bed operation has been selected for the ease and reliability of operation. The main advantage in using SAS is the lower energy requirement, since the heat capacity of the solid is lower and evaporation of water and solvent can be avoided.[6] For large scale CO_2 capture, the ease of regeneration and the stability of the sorbent are important parameters in determining the efficiency, the cost, and the feasibility of a process.[7]

In order to reuse the sorbent, the sorbent needs to be regenerated. The adsorbed CO_2 might be desorbed by (1) increasing the temperature (temperature swing adsorption, TSA) or lowering the partial pressure of CO_2 (pressure swing adsorption, PSA) by applying either (2) vacuum (vacuum swing adsorption, VSA) or (3) introducing purge gas (purge gas adsorption, PGA). Furthermore, these three methods can also be combined to enhance the efficiency of the regeneration process.

Several studies have investigated the effect of the regeneration method on the desorption performance of SAS. Serna-Guerrero et al.[8] found that flow rate of the purge, temperature, and pressure all have a statistically significant influence on the working capacity but that the effect of temperature is dominant with respect to the desorption rate. TSA at 150 °C was found to be the most attractive with the highest CO_2 adsorption loading and the fastest desorption rate.[8] However, urea formation was observed which significantly reduces the available adsorption sites and therefore the lifetime of the sorbent.[9] It is thus important to first investigate the temperature where urea formation starts for each specific sorbent. For instance, the urea formation between PEI and CO_2 occurs above 130 °C.[7]

Regeneration of SAS by PGA under almost isothermal conditions was shown to be an economical and energy efficient

Received: February 15, 2018
Revised: June 26, 2018
Accepted: July 19, 2018
Published: August 1, 2018

DOI: 10.1021/acs.iecr.8b00768
Ind. Eng. Chem. Res. 2018, 57, 11141−11153

alternative in simulations by Pirngruber et al.[10] In general, PSA is mainly superior to TSA due to its lower thermal and mechanical energy demand.[11] Other studies indicate that temperature vacuum swing adsorption (TVSA) might be the most attractive option.[12] Increasing the temperature during the desorption step permits utilization of a weaker vacuum for removal of CO_2 and thus reduced energy requirements for desorption.[13] TVSA conducted at 120 °C and 0.15 bar shortens the CO_2 desorption time to 7.5 min and thus reduces a significant amount of energy penalty, while TSA at 120 °C requires 25 min and VSA at 0.15 bar requires 30 min.[14] Serna-Guerrero et al.[8] showed that a TVSA at 70 °C results in a 13% reduction in working capacity compared to a TSA at 150 °C. The desorption time influences the sorbent cycle time and hence system productivity, equipment size, and ultimately costs of separation.

It is important to note that opposite to CO_2 capture applications, for the case of biogas upgrading the purity of the desorbed CO_2 is not an issue, where in CO_2 capture applications pure CO_2 is preferred for storage or utilization options. In biogas upgrading releasing CO_2 to the environment is not an issue because biogas is considered a renewable source of CO_2.

The objective of this paper is to evaluate, optimize, and compare the various regeneration methods. First, the boundary operating conditions for each regeneration method are identified. Within these constraints, the effect of different process parameters on the degree of desorption and corresponding energy use are determined. Finally, key performance indicators for the most promising regeneration methods are compared.

2. EXPERIMENTAL AND METHODS

2.1. Materials. The sorbent used in this study is a commercial sorbent Lewatit VP OC 1065 from Lanxess. The sorbent has a support of spherical polystyrene beads with primary benzyl amine functional units. The Toth isotherm of this sorbent has been investigated in previous work.[4] The effect of CO_2 pressure and temperature on the isotherm equilibrium loading are shown in Figure 1 and is used to evaluate the desorption performance. Methane is known to be nonreactive with Lewatit.[3,4] H_2S[4] and water[5] do not affect the CO_2 capacity in a negative way. For these reasons it was chosen to represent the biogas by a mixture of CO_2 and nitrogen in this study. In Table 1 more details about the properties of the materials used are given.

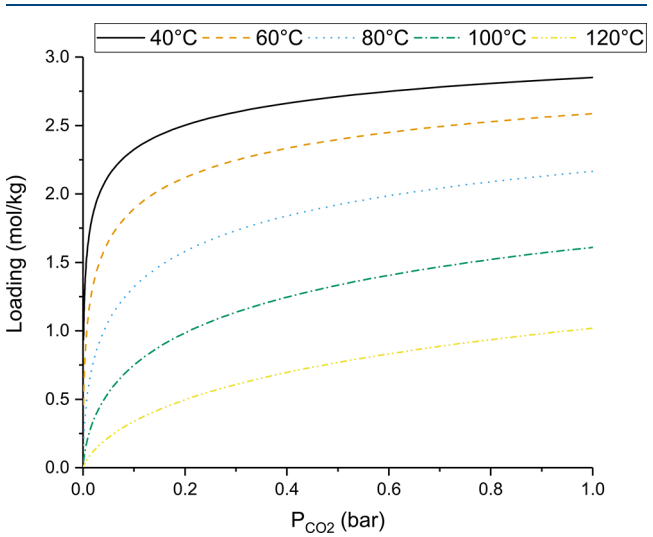

Figure 1. Toth isotherm for lewatit VP OC 1065 produced using isotherm equations of Sutanto et al.[4]

Table 1. Material Properties

symbol	value	unit	meaning	ref
$C_{P,\text{sorbent}}$	1.5	$kJ{\cdot}kg^{-1}{\cdot}K^{-1}$	sorbent heat capacity	15
C_{P,CO_2}	0.85	$kJ{\cdot}kg^{-1}{\cdot}K^{-1}$	CO_2 heat capacity	16
C_{P,N_2}	1.04	$kJ{\cdot}kg^{-1}{\cdot}K^{-1}$	N_2 heat capacity	16
C_{P,O_2}	0.92	$kJ{\cdot}kg^{-1}{\cdot}K^{-1}$	O_2 heat capacity	16
$C_{P,\text{steel}}$	0.50	$kJ{\cdot}kg^{-1}{\cdot}K^{-1}$	steel heat capacity	17
μ_{N2}	1.2×10^{-5}	Pa·s	kinematic viscosity nitrogen	17
d_p	0.7	mm	average particle diameter	18
ρ_{sorbent}	880	$kg{\cdot}m^{-3}$	sorbent density	15
ρ_{steel}	8000	$kg{\cdot}m^{-3}$	density steel	17
ρ_{N2}	1.2	$kg{\cdot}m^{-3}$	density nitrogen	17
MW_{CO_2}	0.044	$kJ{\cdot}mol^{-1}$	molar mass CO_2	
$\Delta_r H$	65	$kJ{\cdot}mol^{-1}$	reaction heat	15

2.2. Equipment. The setup used for the adsorption–desorption experiments consisted of a N_2/CO_2 gas supply, a temperature controlled reactor, and CO_2 analysis equipment. A simplified sketch of the setup is shown in Figure 2. This setup can be operated at different temperatures, using a water bath (Julabo F32/F25) or electrical heating (600W heat tracing controlled by Eurotherm 2132). The pressure can be altered from atmospheric pressure to reduced pressures using a vacuum pump (Vacuubrand PC-510NT).

The fixed bed reactor has a diameter of 13 mm and a length of 600 mm. The fixed bed reactor was filled with 30 g of wet Lewatit sorbent for all experiments. This equals about 19 g of dry sorbent, which is the amount used in the calculations of the sorbent loading. The location of the adsorbent bed in the reactor is changed by a spacer such that a K-type thermocouple is in the axial and radial center of the bed (T_{bed} in the Results and Discussion section). Another K-type thermocouple is placed at the outside reactor wall (T_{wall} in the Results and Discussion section).

High purity (Grade 5.0) CO_2 and N_2 were used in the experiments and the flow rates were controlled with Brooks mass flow controllers (SLA 5850 series). The reactor outlet stream can be diluted with nitrogen, so that the CO_2 concentration is in the measurement range of the CO_2 gas analyzer and a constant flow through the vacuum pump—if operational—is maintained. The concentration of CO_2 in the outlet stream was measured with a CO_2 infrared gas analyzer (Sick Maihak S700) with range of 0–50% and a detection limit of 0.5%. The relative humidity of the gas can be analyzed using three humidity analyzers installed before and after the reactor, respectively, and after the CO_2 analyzer.

2.3. Procedure. The fresh sorbent was pretreated by heating to 150 °C under nitrogen flow before the start of the experimental series. Thereby, any preadsorbed CO_2, H_2O, or other components were removed. Each experimental cycle consisted of three steps: (1) adsorption, (2) desorption, and (3) regeneration of the sorbent. For all experimental cycles, adsorption was performed at 45% CO_2 at atmospheric pressure, 40 °C, and with a total feed gas flow of 215 N

DOI: 10.1021/acs.iecr.8b00768
Ind. Eng. Chem. Res. 2018, 57, 11141–11153

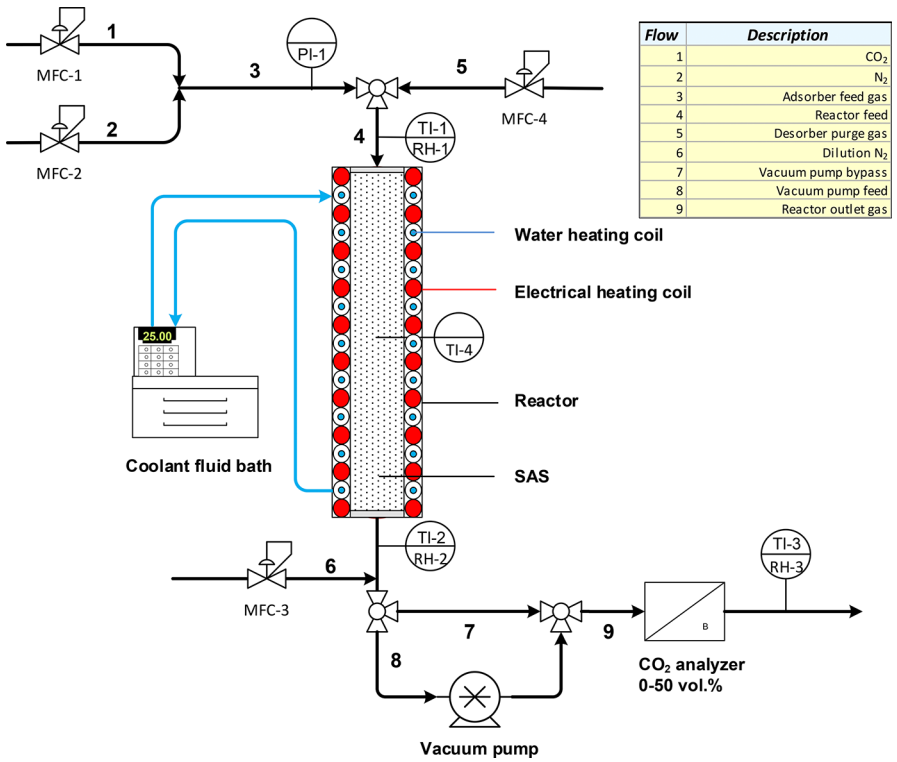

Figure 2. Experimental setup for fixed bed experiments of CO_2 capture.

mL/min. When the measured outlet concentration of CO_2 was equal to the inlet concentration, the adsorption step was stopped. The adsorption loading of the sorbent is calculated by integrating the inlet molar flow of CO_2 and subtracting the integrated outlet molar flow of CO_2. For the desorption loading, the integrated outlet molar flow of CO_2 is subtracted from the adsorption loading.

The procedure of the desorption step is dependent on the chosen method of desorption. For the temperature swing, the pressure swing, and the combined pressure−temperature swing experiments, the reactor inlet was closed after ending the adsorption step. Next, the pressure was reduced using the vacuum pump and/or the reactor was heated. When using combined pressure and temperature swing, the pressure was reduced before the reactor was heated. If a nitrogen or air purge was used, the purge flow was started after the adsorption was stopped and the heating was started simultaneously. When a reduced overall pressure was used, first the reactor was evacuated and next the purge flow was started. Desorption was stopped when no CO_2 was detected in the outflow by the analyzer. After the desorption step, the sorbent was fully regenerated at 150 °C under nitrogen flow in order to make sure that all adsorbed components were removed and the sorbent was clean and ready for the next adsorption.

2.4. Error Analysis. All experiments have been performed with the same sample of sorbent. This allowed quick successive experimentation and also gave an indication of degradation of the sorbent. In Figure 3 the adsorption loadings of all experiments are presented. The average of the experimental equilibrium adsorption loading (40%CO_2 40 °C) is 2.6 ± 0.1 mol/kg. All shown errors in this article are defined via one standard deviation. The result in Figure 3 shows that the reproducibility of the adsorption experiments is good. The first two experiments in Figure 3 show a lower adsorption loading.

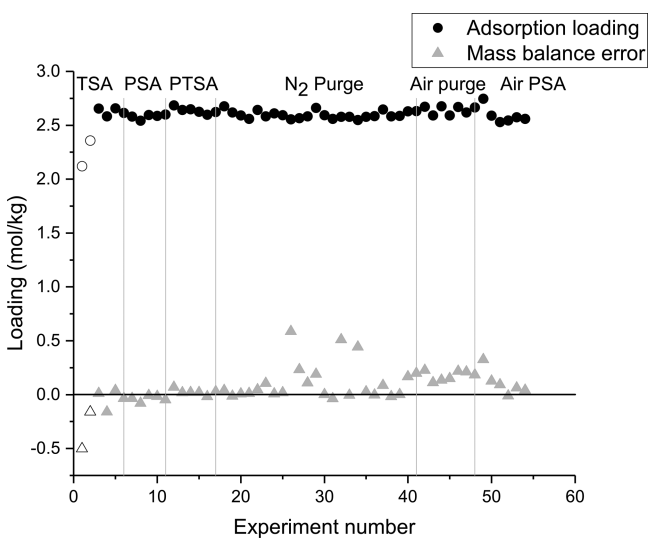

Figure 3. Adsorption equilibrium loading (sphere) and loading after regeneration (triangle) for all experiments performed.

Note that also the loading after regeneration is below zero. Therefore, it is concluded that the sorbent was not completely empty before the adsorption was started. Within these 55 experiments, no signs of degradation have been observed within the experimental error. Performing a *t* test at 95% significance level using the first 27 and last 28 experiments showed that statistically these two group have the same mean value.

Another error analysis on the experiments can be made by examining the mass balance. In Figure 3 the mass balance closure is expressed as the loading after regeneration. Since all adsorbed CO_2 should be removed in the combined desorption and regeneration step, the theoretical loading after regener-

DOI: 10.1021/acs.iecr.8b00768
Ind. Eng. Chem. Res. 2018, 57, 11141−11153

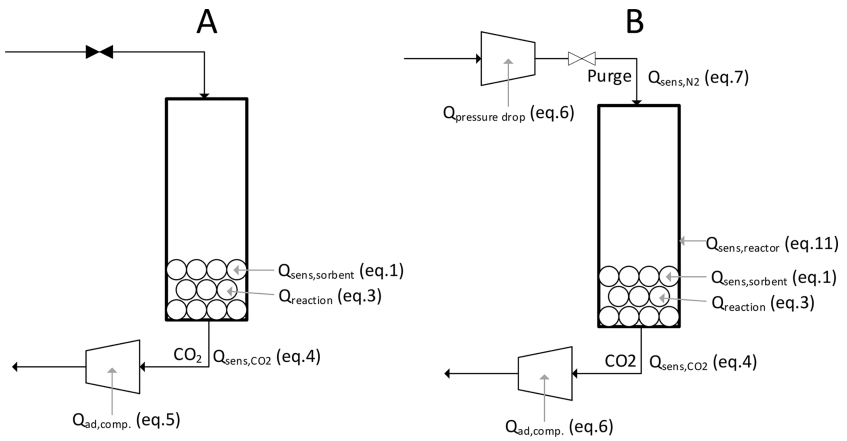

Figure 4. Overview of energy flows included in the calculations. (A) For no purge (Figure 6) and (B) for purge calculations (Figure 14).

ation should be zero. The average error on the mass balance is 0.1 ± 0.2 mol/kg.

In general, it is noted that the experiments at lower desorption temperatures have a larger error. For example, the three points in the N_2 purge section with an error around 0.5 mol/kg are found in all experiments performed at 40 °C desorption temperature. Because of the lower desorption temperature the desorption rate is lower, resulting in CO_2 outlet concentrations at/below the detection limit of the CO_2 analyzer. Consequently, the CO_2 removed from the reactor is not detected.

The set of air purge experiments was performed using instrumental air. During a measurement it was noted that the CO_2 content in the instrumental air was fluctuating between 50 and 250 ppm. Therefore, a value of 150 ppm in the instrumental air was assumed for the calculations. However, because the CO_2 content is estimated, the error in the CO_2 loading after regeneration is increased as is clearly visible in Figure 3.

2.5. Energy Calculations. In order to evaluate the regeneration of solid amine sorbent in more detail energy calculations have been performed. The total amount of energy needed for desorption has been calculated for a selection of experiments. In the section below the equations needed are discussed in more detail, and the material properties are given in Table 1.

2.5.1. Calculations for Experiments without Purge Flow. In the calculations for experiments without purge flow the sensible heat of the sorbent and the produced CO_2 are included. Next to that, the reaction heat and—if necessary—the energy for adiabatic compression are added. In Figure 4A an overview of the energy flows included is given.

First of all, the sensible heat of the sorbent ($Q_{\text{sensible,sorbent}}$ [J·$kg_{CO_2}^{-1}$]) is calculated using eq 1, where $T_{\text{desorption}}$ and $T_{\text{adsorption}}$ are the desorption and adsorption temperatures, respectively.

$$Q_{\text{sensible,sorbent}} = m_{\text{sorbent}} \cdot C_{P,\text{sorbent}} \cdot (T_{\text{desorption}} - T_{\text{adsorption}}) \quad (1)$$

The sorbent mass m_{sorbent} is calculated by the amount of dry sorbent mass needed to capture 1 kg of CO_2 using the molar mass of CO_2 MW_{CO_2} and the working capacity Δq_{exp} of the corresponding experiment:

$$m_{\text{sorbent}} = \frac{1}{\Delta q_{\text{exp}} \cdot MW_{CO_2}} \quad (2)$$

Because the desorption reaction of the CO_2 from the amine is endothermic, energy is required for the reaction. The amount of energy required per kg of CO_2 is calculated by dividing the reaction heat $\Delta_r H$ by the molar mass MW_{CO_2}:

$$Q_{\text{reactionheat}} = \frac{\Delta_r H}{MW_{CO_2}} \quad (3)$$

The sensible heat of the CO_2 released is calculated by

$$Q_{\text{sensible,CO2}} = C_{P,CO_2} \cdot (T_{\text{desorption}} - T_{\text{adsorption}}) \quad (4)$$

In the case of a pressure swing regeneration, energy is required to create a reduced pressure in the reactor during desorption. Adiabatic compression[19] is assumed, and the required energy is calculated by eq 5 for the cases without purge flow. The efficiency of compression η is assumed to be 0.75, and the ratio of C_p/C_v is k = 1.3.[20] In eq 5, P_1 is the suction pressure of the compressor, whereas P_2 is the discharge pressure which is assumed to be 1 bar.

$$Q_{\text{adiabaticcompression}} = \frac{1}{\eta} \cdot \frac{k}{k+1} \cdot \frac{1}{MW_{CO_2}} \cdot RT_{\text{desorption}} \cdot \left[\left(\frac{P_2}{P_1} \right)^{k-1/k} - 1 \right] \quad (5)$$

2.5.2. Calculations for Experiments with Purge Flow. The energy calculations for the cases including purge flow are presented in Figure 4B. The energy flows calculated in the section below are expressed in Joule per desorption step. In Figure 14 the energy flow are expressed in J·$kg_{CO_2}^{-1}$ by dividing the calculated energy flows from this section by the amount of CO_2 produced per adsorption−desorption cycle.

For the cases including a purge gas flow, eq 5 changes slightly because the amount of flow has to be incorporated. The flow of the purge gas and the produced CO_2 are included. Again adiabatic compression is assumed and calculated by[19]

DOI: 10.1021/acs.iecr.8b00768
Ind. Eng. Chem. Res. 2018, 57, 11141−11153

$$Q_{\text{ad.comp.}} = \frac{1}{\eta}\cdot\frac{k}{k+1}\cdot\phi_{\text{mole,CO}_2}\left(1+\frac{1}{\text{ratio}(\text{CO}_2/\text{purge})}\right)\cdot RT_{\text{des}}\cdot\left[\left(\frac{P_2}{P_1}\right)^{k-1/k}-1\right]\cdot t_{\text{des}} \quad (6)$$

In eq 6, P_1 is the suction pressure of the compressor whereas P_2 is the discharge pressure. In the case of gas compression for creating reduced pressure ($Q_{\text{ad,comp}}$ in Figure 4B), P_2 is considered to be 1 bar and P_1 is the pressure of the corresponding experiment. In the case of gas compression to overcome the pressure drop over the adsorbent bed ($Q_{\text{pressuredrop}}$ in Figure 4B), P_2 is ΔP + 1 and P_1 is assumed to 1 bar. The pressure drop over the bed (ΔP) is calculated by the Ergun equation.[21] The length of the reactor is determined using a short-cut design method; more details can be found in Section 3.4.1. The sensible heat of the purge flow (in eq 7 N_2 is used as example) can be calculated using eq 7.

$$Q_{\text{sensible,N}_2} = \phi_{v,\text{purge}}\rho_{\text{N}_2}\cdot C_{P,\text{N2}}\cdot(T_{\text{desorption}} - T_{\text{adsorption}}) \quad (7)$$

The amount of purge flow $\phi_{v,\text{purge}}$ is determined by keeping the ratio between CO_2 and the purge medium constant to the experimental ratio. The importance of this is shown in Section 3.3.4. The amount of CO_2 flow (see eq 8) during desorption is equal to the amount of CO_2 fed in adsorption because capture efficiency is assumed to be 100% in the short-cut design method.

$$\phi_{\text{mole,CO}_2} = \frac{\phi_{V,\text{feed}}P_0}{RT_0}x_{\text{CO}_2} \quad (8)$$

$$\phi_{v,\text{purge}} = \frac{\phi_{\text{mole,CO}_2}}{\text{Experimental ratio}(\text{CO}_2/\text{purge})}\cdot\frac{RT}{P} \quad (9)$$

The sensible heat of the reactor is estimated by calculating the amount of steel needed—see eq 10—and the eq 11. In eq 10 the d_s and L_r are the diameter of the shell and length of the reactor, respectively. n_t and d_t are the number and the diameter of the tubes. Calculations for the dimensions of the reactor are discussed in Section 3.4.1. The wall thicknesses of the shell wt_s and the tubes wt_t are assumed to be 10 mm and 0.8 mm, respectively.

$$m_{\text{steel}} = (m_{\text{shell}} + 2\cdot m_{\text{bottom/top}} + n_t\cdot m_{\text{tube}})\cdot\rho_{\text{steel}} = \left(\pi d_s L_r \text{wt}_s + 2\frac{1}{4}\pi d_s^2 \text{wt}_s + n_t\pi d_t L_r \text{wt}_t\right)\cdot\rho_{\text{steel}} \quad (10)$$

$$Q_{\text{sensible,reactor}} = m_{\text{steel}}\cdot C_{P,\text{steel}}\cdot(T_{\text{desorption}} - T_{\text{adsorption}}) \quad (11)$$

3. RESULTS AND DISCUSSION

3.1. Stability of SAS. The first step is to check the temperature stability of the sorbent to set the boundaries of utilized process conditions. The sorbent manufacturer recommends an operating temperature in the range of 20 °C to 100 °C[18] and several studies have reported urea-bridge formation in the presence of CO_2 at high temperature.[7,22] Because air is the cheapest option of purge gas, a quick test of oxidative stability of the sorbent was carried out at 80 and 100 °C for 1 h, which showed degradation of 5−6% of capacity, but insignificant degradation at 60 °C. These results are in line with findings of Yu et al.[22] that show that in the presence of oxygen the sorbent is only stable up to approximately 70 °C due to oxidative degradation. However, without the presence of CO_2 and O_2, the thermal stability of the sorbent can be maintained up to 150 °C. In the presence of CO_2 the sorbent stability/regenerability is less well studied but appears to be stable up to 130 °C, above which urea formation might occur.[22,23] The option of using CO_2 as purge gas was also considered. However, since the purity of CO_2-rich product gas is not an issue in biogas upgrading, the higher probability of urea formation, and lower working capacities, this option is considered less attractive for the biogas case and hence left out in this study.

From stability tests, it was decided to perform TSA at a maximum temperature of 120 °C when CO_2 is present. When air is used as purge gas, the temperature is limited to 60 °C to prevent oxidative degradation. So far, no significant degradation has been observed or reported for regeneration methods using reduced absolute pressure.

3.2. Desorption without Purge Flow. First, experiments without purge flow were executed, and the results are shown in Figure 5. The 30 min working capacity is defined as the difference between the adsorption equilibrium capacity and desorption loading after 30 min of desorption. The final working capacity is defined as the difference between the adsorption loading and the loading at the end of the desorption step (t > 40 min). By integration of the outlet CO_2 mole flow during the regeneration step the residual loading is found.

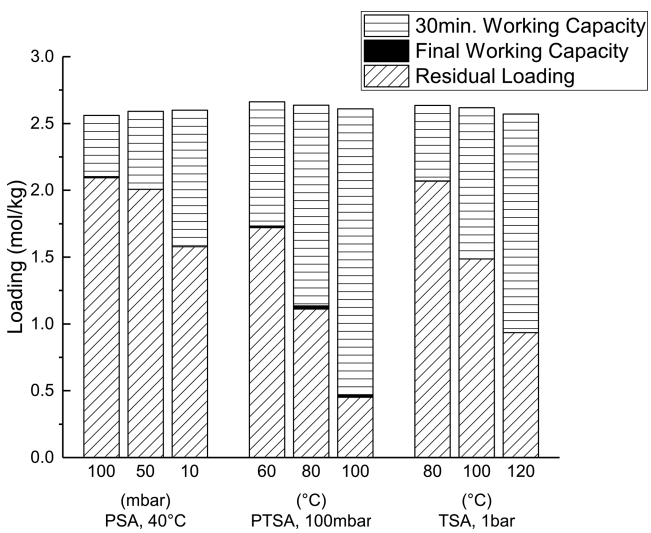

Figure 5. Residual CO_2 loading (mol/kg) on the sorbent after 30 min and at the end of the desorption step without purge flow. Desorption was varied between the methods: PSA was performed at 40 °C, PTSA at 100 mbar, and TSA at 1 bar.

Pure pressure swing experiments have been performed at the adsorption temperature of 40 °C. This would enable a more or less isothermal adsorption/desorption process. This method of desorption is not very effective, as shown in Figure 5. Even at a low system pressure of 10 mbar, only 40% of the adsorption loading is removed during desorption. Increasing the temperature is more effective in cleaning the sorbent as is shown by the temperature swing experiments in Figure 5. This observation is in line with Lewatit VP OC 1065 being a chemical sorbent, where energy is needed to break the chemical bond between the sorbent and absorbed species. The

DOI: 10.1021/acs.iecr.8b00768
Ind. Eng. Chem. Res. 2018, 57, 11141−11153

effect of temperature is larger than the effect of pressure due to the shape of the isotherm for the sorbent used (see Figure 1). The isotherm is very steep in the region of low pressure of CO_2 (<5 kPa).[4] Consequently, the system pressure must be lowered to a significantly lower pressure (<1 Pa) in order to evacuate the sorbent completely at a temperature of 40 °C. Combination of pressure and temperature swing (PTSA) leads to higher working capacities at lower temperatures and higher pressure compared to pure TSA of PSA.

In order to get more insight in the most optimal desorption method, a comparison of energy consumptions is made. The required sensible heat for the sorbent and the produced CO_2 are calculated. The compression cost is estimated by adiabatic compression of the produced CO_2. Using the experimental determined working capacities from Figure 5, the amount of sorbent required to produce one kilogram of CO_2 per cycle is calculated. A more detailed description of these calculations can be found in Section 2.5.1.

The energy comparison showed a more favorable result for the PSA as shown in Figure 6, merely as a result of the fact that

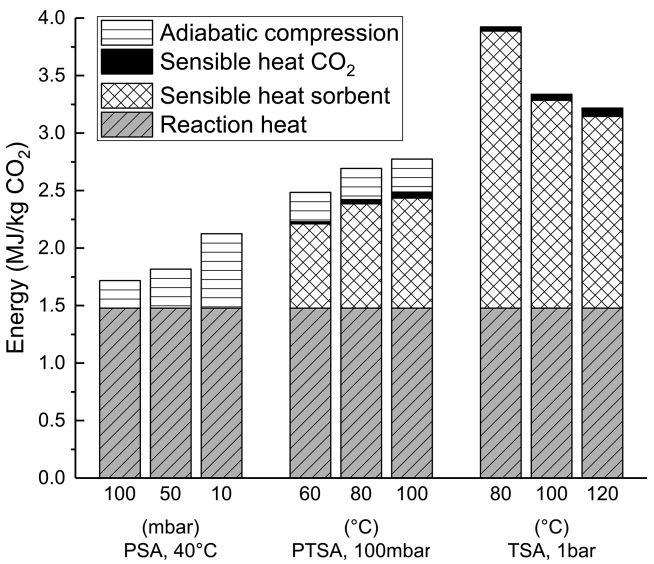

Figure 6. Energy use (MJ/kg CO_2) of the cases presented in Figure 5 based on the reaction heat, the adiabatic compression, and the sensible heat of the sorbent and the produced CO_2.

for PSA energy is only added to the product while for TSA energy is added to the product and the sorbent. Therefore, the optimum based on energy usage will be found for a PSA case with low-pressure difference between the adsorption and the desorption step. However, this case can be considered impractical since it will have a very low working capacity and therefore a lot of adsorption/desorption cycles have to be performed to produce one kilogram of CO_2. This leads to larger equipment size and investment costs, for a given capacity of the biogas plant. Consequently, another optimum will be found if more factors (e.g., economic factors) are included in the optimization. Shortly, it can be concluded that temperature swing is needed to reach a noteworthy working capacity and pressure swing can be used to lower the required sensible heat. The trade-off between these is subject of economic optimization depending on cost and availability of utilities.

3.3. Desorption with Purge Gas Flow. Instead of reducing the CO_2 pressure by reducing the system pressure, a purge gas flow can be used to lower the CO_2 partial pressure. An effective purge gas should be inert, abundantly available, and optimally inexpensive. In literature[7,8,15,22] nitrogen is considered an effective purge gas and therefore evaluated in this paper. Alternatively, especially for a larger scale operation, air might be a cheaper purge gas although less inert due to the oxygen content. Emitting CO_2 from biogas to the air is not considered a contribution to CO_2 related global warming as the CO_2 in biogas originates from renewable biomass.

3.3.1. Temperature Effect on Capacity. From the isotherm of Lewatit[4] (see Figure 1), it is clear that an increasing temperature will lead to an increased working capacity. This effect is clearly seen in Figure 7 as the working capacity

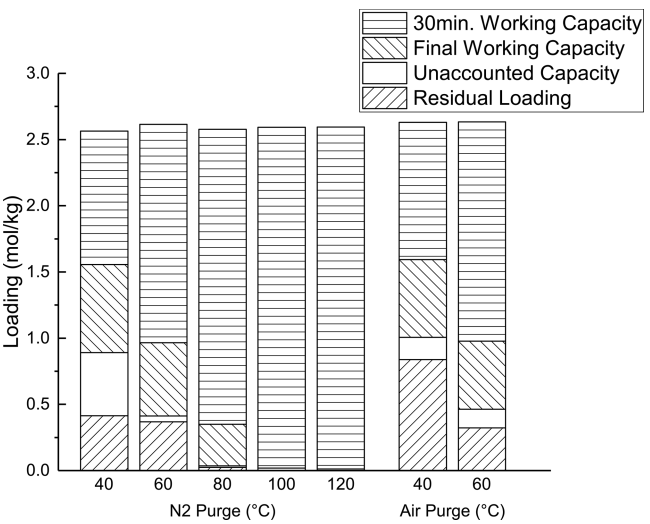

Figure 7. Effect of temperature on residual CO_2 loading on the sorbent after 30 min and at the end of the desorption step with a purge flow of 226 mL/min.

increases from 1 mol/kg at 40 °C to 2.5 mol/kg above 100 °C for both cases after 30 min of desorption. The significant faster desorption above 80 °C is in line with results of Serna-Guerrero et al.[8]

In contrast to what the theory predicts, Figure 7 shows a significant final loading is present for the 40 and 60 °C N_2 purge cases. In Figure 8 it is shown that a kind of equilibrium (at 0.9 mol/kg) is reached for the 40 °C case after 7 h of the desorption. In the next 9 h of the desorption step, no significant (<0.5% CO_2, below detection limit) CO_2 was measured in the outlet of the reactor. In the following regeneration step only 0.4 mol/kg was desorbed although 0.9 mol/kg was expected. In our opinion, the missing 0.5 mol/kg (shown as "unaccounted capacity" in Figure 7) desorbed during the last 9 h of the desorption step. This opinion is supported by the fact that the subsequent adsorption step of the next experiment showed again full adsorption capacity (see Figure 3).

Additionally, in Figure 7 the nitrogen purge is compared with the air purge experiments. As seen, the working capacities after 30 min for the nitrogen purge and air purge are almost equal. Therefore, it can be concluded that the CO_2 present in air does not have a significant effect on the desorption rate in the first 30 min. This hypothesis is confirmed when the average outlet CO_2 molar fraction is calculated (average X_{CO2} = 0.06 for 40 °C N_2 purge case), and it is noted that the average outlet concentration is not significantly changed by 400 ppm

DOI: 10.1021/acs.iecr.8b00768
Ind. Eng. Chem. Res. 2018, 57, 11141−11153

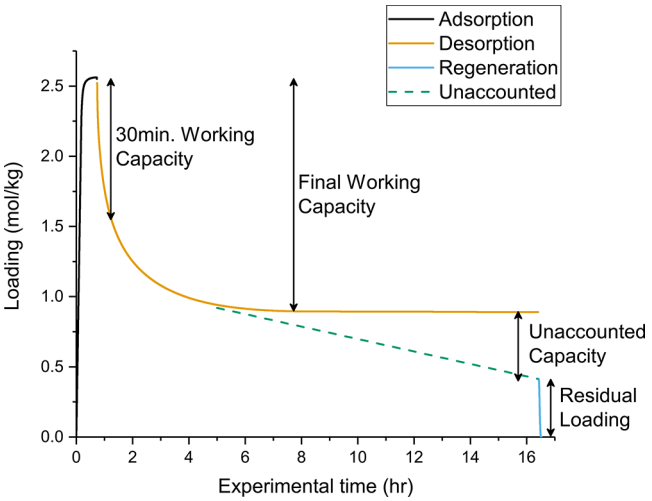

Figure 8. Experimental loading versus time for the 40 °C, 226 N mL/min N_2 purge case. The dashed line illustrates the decrease in loading when the CO_2 concentration was below the detection limit of the analyzer.

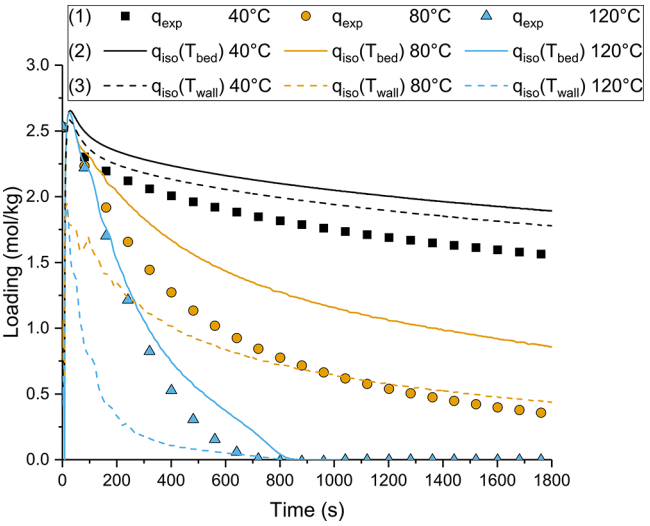

Figure 9. Experimental bed-average loading (1) at 40, 80, and 120 °C and 226 N mL/min N_2 purge. Additionally, the Toth isotherm values evaluated at the outlet CO_2 concentration and the bed temperature (2) or the outside wall temperature (3) are shown.

(X_{CO2} = 0.0004) of CO_2 in air. Additionally, it is shown in Figure 6 that the CO_2 in air has an significant effect on the final loading. This is predicted by theory, since the isotherm value at 150 ppm of CO_2 in the instrument air used and 40 °C is 0.5 mol/kg. However, this also shows that the presented final loading is not the equilibrium loading. Note that the unaccounted capacity is small for the 40 °C air purge experiment because it was stopped after 3.8 h of desorption when the CO_2 outlet concentration was below the detection limit, instead of running the experiment 17 h for the 40 °C nitrogen purge.

3.3.2. Temperature Effect on Desorption Rate. In Figure 7 it is also observed that the desorption *rate* is increasing with temperature since the difference between the 30 min and the final working capacity is reduced with increasing temperature. Desorption of CO_2 will only happen when the equilibrium loading at the local conditions is lower than the actual loading. This is analyzed in Figure 9 by plotting the bed-average experimental loading (1) versus time. The experimental loading is compared to the Toth isotherm loading, evaluated at the CO_2 concentration at the reactor outlet and the bed temperature (2), respectively, and the outside wall temperature (3).

In Figure 9 is shown that both the isotherm lines lay above the experimental line for the 40 °C experiment. Based on this observation desorption is not expected. However, the isotherm lines are evaluated at the CO_2 outlet concentration, which is the highest CO_2 concentration in the column. Because CO_2-free nitrogen is entering the column, the local CO_2 concentration will be lower, and thus the local isotherm value will be lower. Therefore, locally desorption can happen. Moreover, the experimental loading is a column-averaged loading. Seeing that desorption will happen in the beginning of the column first, the actual local experimental loading will be lower in the beginning and higher at the end of the column. For that reason, desorption is possible at the end of the column despite that the isotherm lines are higher than the experimental line. This is supported by the fact that the isotherm is extremely favorable for adsorption, and it will be unfavorable for desorption. This will lead to a flat mass transfer zone as described by Ruthven[24] and Seader et al.[25]

On the other hand, the experimental loading for the 120 °C case is higher than the isotherm line evaluated on the wall temperature for all times (see Figure 9). This means that, at least around the wall, desorption is possible along the whole length of the column. Therefore, the desorption front will be less distinct for the 120 °C experiments. For the reason that desorption is possibly occurring in a larger fraction of the column compared to the 40 °C case the desorption rate will be higher for the 120 °C case. Additionally, the isotherm line evaluated at the bed temperature suggests that the experimental loading is in equilibrium with the outlet gas concentration.

The large difference in isotherm values for the wall and the bed shown in Figure 9 for the 120 °C case is a result of the large radial temperature gradient of 35 °C seen during the experiments. A large radial temperature gradient is present due to low thermal conductivity of the sorbent. Consequently, there might be a large radial gradient in local loading. For example, the sorbent might be empty at the wall but still contain CO_2 in the center of the bed. The low thermal conductivity of the sorbent is an important factor for the design of an up-scaled system because too large column diameters might lead to large radial temperature gradients. As a result, large temperature gradients might cause excessive regeneration times to remove all CO_2 from the column and thereby cause lower column productivities.

The above results suggest that desorption rate is strongly influenced by the equilibrium between the gas and the adsorbed phase. For the 40 °C case this seems to be more locally at the desorption front where for the 120 °C this seems to be along the length of the whole column.

3.3.3. Equilibrium Model. The strong influence of the equilibrium between gas and adsorbed phase is investigated in more detail by use of an equilibrium PFR model of the column. The gas phase has been modeled as an ideal PFR assuming local equilibrium with the adsorbed phase as shown in eq 12. In this equation is C_g (mol·m^{-3}) the gas phase concentration, q_e and q (mol·kg^{-1}) the equilibrium sorbent loading and the

DOI: 10.1021/acs.iecr.8b00768
Ind. Eng. Chem. Res. 2018, 57, 11141−11153

actual sorbent loading, respectively, u_g ($m \cdot s^{-1}$) the superficial gas velocity, ε (−) the bed voidage, and ρ_s ($kg \cdot m^{-3}$) the sorbent density (see also Table 2).

$$\frac{\partial C_g}{\partial t} = \frac{u_g}{\varepsilon}\frac{\partial C_g}{\partial z} - k_1(q_e - q)\rho_s\frac{(1-\varepsilon)}{\varepsilon} \quad (12)$$

Table 2. Values of Parameters in the Equilibrium Model

symbol	value	unit	meaning
ε	0.38	−	bed voidage
k_1	1×10^9	s^{-1}	linear driving force constant
ρ_s	880	$kg \cdot m^{-3}$	sorbent density

The mass transfer between the gas and the solid phase has been modeled using the linear driving force model with a sufficient large linear driving force constant (k_1, eq 13). In this way, local equilibrium is ensured between the gas and the solid phase.

$$\frac{\partial q}{\partial t} = k_1(q_e - q) \quad (13)$$

The experimental increase in temperature is approached using a segmented linear temperature increase as shown in Figure 10B. The equations used are shown in eq 14 when the temperature is increasing with slope $\frac{\Delta T}{\Delta t}$ determined from the experimental temperature increase and with eq 15 when the temperature is constant. Using this method, the experimental temperature profile is approached without extensive modeling of heat transfer phenomena.

$$\frac{\partial T}{\partial t} = \frac{\Delta T}{\Delta t} \quad \text{for } t < t(T_{constant}) \quad (14)$$

$$\frac{\partial T}{\partial t} = 0 \quad \text{for } t > t(T_{constant}) \quad (15)$$

The equations are solved using the ODE15s solver in Matlab. The differential $\frac{\partial C_g}{\partial z}$ is manually discretized, while the differential $\frac{\partial C_g}{\partial t}$ is solved by the ODE15s solver.

In Figure 10 it is shown that the prediction of the trend in loading by the equilibrium PFR model matches with the experimental trend. Hence, the desorption rate is strongly influenced by the equilibrium between the gas and the solid phase as hypothesized in the previous section. Because the isotherm is strongly dependent on temperature also the desorption rate depends strongly on temperature. This implicates that heat transfer is an important parameter when designing the adsorption/desorption system. Better heat transfer will raise the reactor temperature faster and thereby increase the desorption rate resulting is smaller equipment.

In Figure 10A it is seen that the model predicts the two extremes in temperatures (40 and 120 °C) the best. Surprisingly, the predictions for the temperatures in between are worse. It is expected that slight imperfections of the isotherm might influence the model results. Additionally, the influence of the produced CO_2 on the gas velocity is not taken into account in the modeling. The desorption rate might be under-predicted for this reason since the gas velocity will increase when the produced CO_2 is taken into account.

It can be concluded that the capacity of the sorbent as a function of temperature is strongly influenced by the isotherm. At 40 and 60 °C the desorption is too slow to reach equilibrium without excessive (above 3 h) regeneration times. Above 100 °C the sorbent is completely clean within half an hour of desorption.

3.3.4. Effect of Purge Gas Flow Rate. The effect of purge gas flow rate also depends on the temperature, as shown in Figure 11. While at 60 °C there is a significant influence of the purge flow, at 120 °C there is only a minimal increase in desorption rate. For the 60 °C experiments, especially in the first 30 min a strong effect of flow on the desorption rate is seen. In the following 2 h of the experiment it seems that the desorption rates have the same order of magnitude, because the difference between the 30 min loading and the residual loading is almost independent of the flow rate.

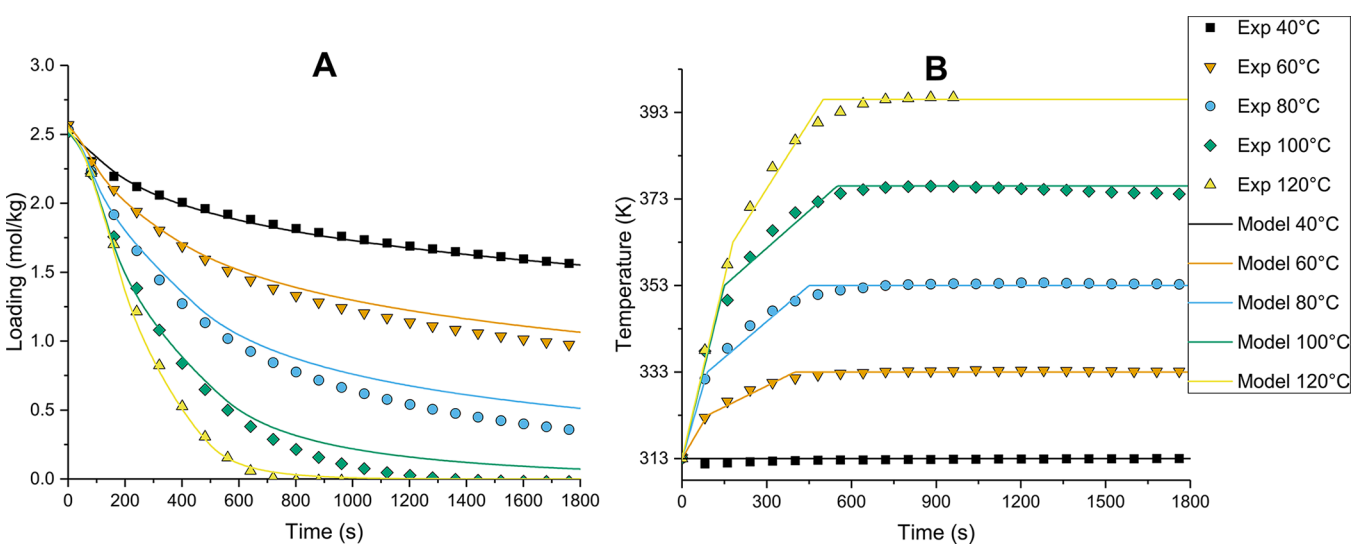

Figure 10. Experimental loading (A) and temperature (B) and predicted values by the equilibrium model for the nitrogen purge experiments presented in Figure 7. The figures have a shared legend.

DOI: 10.1021/acs.iecr.8b00768
Ind. Eng. Chem. Res. 2018, 57, 11141−11153

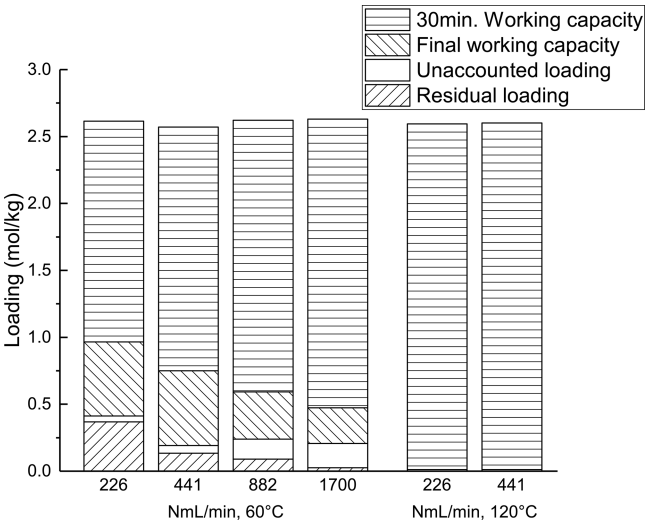

Figure 11. Effect of purge gas flow rate [NmL/min] and temperature on residual CO_2 loading on the sorbent after 30 min and at the end of the desorption step at 60 and 120 °C.

In Figure 12 this effect is also clearly visible, and in the first 600 s the desorption is influenced by the flow rate while after

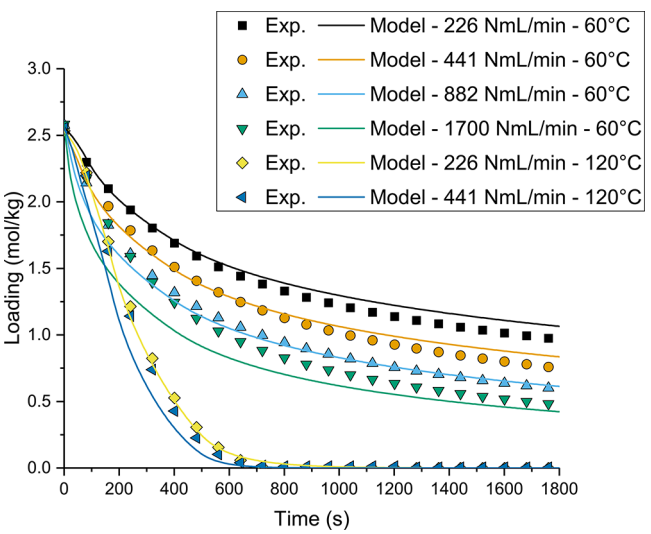

Figure 12. Experimental loading and predicted values by the equilibrium model for the nitrogen purge experiments presented in Figure 11.

600 s the desorption rate appears to be the same for all flow rates. This shows that in the first 600 s the desorption rate is strongly influenced by the gas concentration. Desorption of CO_2 will only happen when the equilibrium loading at the local conditions is lower than the actual loading. Initially, the desorption rate will be higher for a higher flow rate because the gas concentration is lower. Therefore, a larger fraction of the adsorbed CO_2 can desorb from the bed before reaching equilibrium between the gas and adsorbed phase, resulting in a lower sorbent loading. After 600 s, albeit having a lower gas concentration, also the local loading is lower for the higher flow rate. Therefore, after 600 s the effect of a lower gas concentration at higher flow rate is canceled by the effect of lower local loading. Consequently, the desorption rate appears to be same.

For the high temperature experiments, it is shown in Figure 12 that the difference in desorption rates is minimal. In view of the high desorption rates, the CO_2 concentrations are high (>25%) during the experiment. Because of the high temperature and CO_2 concentration, the isotherm is in the flat region (see Figure 1). Consequently, the effect of a reduction in CO_2 concentration is small and therefore the influence of flow is minimized. Additionally, Figure 10B indicates that after 700 s the sorbent reaches 120 °C whereas the sorbent is also fully regenerated after 700 s. Consequently, the desorption rate might be increased by increasing the heating rate. It supports the idea that ensuring good heat transfer to the sorbent is important when designing a SAS CO_2 removal system.

3.3.5. Effect of System Pressure. Since the maximum temperature using air purge is limited to 60 °C due to oxidative degradation,[22] the effect of lowering the system pressure while using an air purge is investigated. Due to lower CO_2 pressure, a lower final loading is expected for a lower system pressure. Comparing the residual loadings in Figure 13, this effect can be clearly seen.

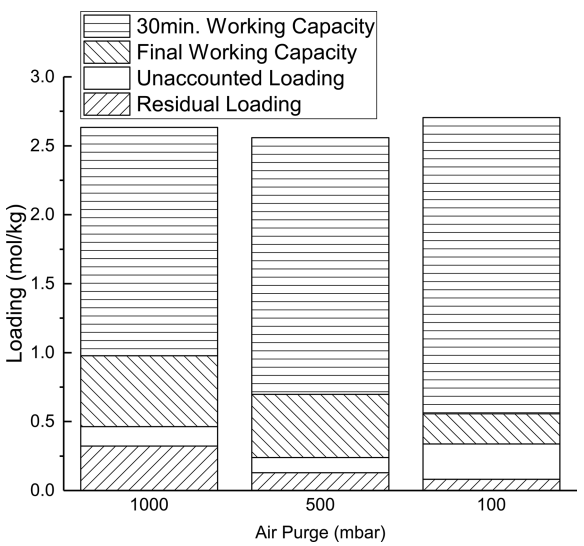

Figure 13. Effect of pressure on residual CO_2 loading on the sorbent after 30 min and at the end of the desorption step at temperature of 60 °C and an air-purge flow of 226 N mL/min.

Next to the lower final working capacity, the difference between the working capacity after 30 min and at the end of the desorption step is also reduced with decreasing pressure. This increase in desorption rate might be due to enhanced mass transfer as a result of an increased diffusivity of CO_2. Additionally, since the volume flow is set in normal liters per minute and held constant during the experiments, the gas velocity will increase with decreasing pressure. This will increase both the mass transfer from the particle to the bulk and the CO_2 removal from the reactor. In general, it can be said that the working capacity and the desorption rate are increased with decreasing pressure. However, additional optimization (e.g., economics) has to be performed in order to determine the most optimal desorption case.

3.4. Evaluating Regeneration Options. In the previous section, the working capacity for different options of regeneration have been shown. As mentioned before, selection of the most optimal conditions based on working capacity and desorption rate is not trivial. Here, an energy comparison is

DOI: 10.1021/acs.iecr.8b00768
Ind. Eng. Chem. Res. 2018, 57, 11141−11153

Table 3. Operating Conditions of the Selected Desorption Methods

	case	pressure [bar]	desorption temperature [°C]	exp. 30 min working capacity [mol/kg]	30 min avg. CO_2 concentration for 226 N mL/min experiments [mol CO_2/mol N_2]
1	air purge	0.1	60	2.2	0.14
2	air purge	1	60	1.7	0.11
3	nitrogen purge	1	60	1.7	0.11
4	nitrogen purge	1	80	2.2	0.14
5	nitrogen purge	1	100	2.6	0.16
6	PTSA	0.1	80	1.5	n/a

performed, taking as point of departure the CO_2 removal for a 1000 N m^3/h biogas plant. Three cases with a working capacity around 1.6 mol/kg after 30 min are selected. Experimental results are used from the following experiments: nitrogen (1) and air purge (2) at 60 °C and 226 N mL/min and PTSA at 80 °C (3). To see the effect of reduced pressure under flow conditions, the air purge at 60 °C and 100 mbar (4) is added. The effect of temperature is investigated by adding the nitrogen purge experiments at 80 (5) and 100 °C (6). An overview of the experimental conditions used in the evaluation below can be seen in Table 3.

3.4.1. Design Method. In order to include the energy loss by the pressure drop over the sorbent bed, a short-cut design of a large scale adsorption column has been made. The column has been designed for the case of 1000 N m^3 h^{-1} of biogas containing 45% of CO_2; for more details see Table 4. For the design it is assumed that all of the CO_2 is captured during 30 min of adsorption. The possible broadening of the mass transfer zone and early breakthrough because of incomplete regeneration are not taken into account. However, in a more detailed design, it should be taken into account since it might affect the realized working capacity and thereby the equipment size.

Table 4. Design Specifications and Assumptions Used for the Short-Cut Design

meaning	symbol	value	unit
biogas flow	$\phi_{V,feed}$	1000	$N{\cdot}m^3{\cdot}h^{-1}$
CO_2 fraction	x_{CO_2}	0.45	–
CO_2 capture capacity	–	872	$kg_{CO_2}{\cdot}h^{-1}$
temperature adsorption	T_{ads}	40	°C
time adsorption and desorption	t_{ads}/t_{des}	1800	s
gas velocity during adsorption	u_g	0.25	$m{\cdot}s^{-1}$

The reactor is designed as a multitubular reactor where the diameter of the tubes is equal to the experimental diameter (13 mm). Thereby, heat transfer into the reactor is similar to the experimental heat transfer phenomena, ensuring the experimental working capacity can be reached in the designed column. The total area for gas flow is calculated using the flow of biogas and assuming a gas velocity of 0.25 m/s in the tubes during adsorption; see eq 16. The gas velocity during adsorption is fixed to be able to specify the other two independent variables, the length of column and diameter of the shell.

$$A_r = \frac{\phi_{V,feed}}{u_g} \tag{16}$$

The number of tubes n_t is determined by dividing the total area for gas flow by the area of one tube.

$$n_t = \frac{A_r}{\frac{1}{4}\pi d_t^2} \tag{17}$$

The area A_s of the shell is determined by eq 18. From the area of the shell the shell diameter can be determined.

$$\frac{A_r}{A_s} = 0.9\left[\frac{d_t}{1.25 d_t}\right]^2 \tag{18}$$

The amount of sorbent $m_{sorbent}$ is calculated using the experimentally determined 30 min working capacity Δq_{exp} and the mole flow of CO_2; see eq 8. The mole flow of CO_2 is determined from the biogas feed flow and the fraction of CO_2 as shown in eq 8.

$$m_{sorbent} = \frac{\phi_{mole,CO_2} t_{ads}}{\Delta q_{exp}} \tag{19}$$

Using the sorbent mass and the bulk density of the sorbent, the length of the reactor can be calculated. It is assumed that the reactor has the same dimensions as the sorbent bed and no dead spaces are present in the reactor.

$$L_r = \frac{m_{sorbent}}{\rho_{sorbent}(1-\varepsilon)A_r} \tag{20}$$

The amount of purge flow is calculated such that the average ratio of N_2 and CO_2 in the designed situation is equal to the average ratio between N_2 and CO_2 in the corresponding experiment; see eq 9. The reason for this is that desorption is strongly influenced by local equilibrium (as shown in Section 3.3.3) and therefore the concentration of CO_2 in the outlet is an important factor to be considered. Not included in the evaluation is the coadsorption of water, although depending on the ratio of working capacity for H_2O and CO_2, the energy penalty might be significant. If this ratio is one, the penalty of desorption heat of H_2O is already 0.98 MJ/kg CO_2. However, assuming 100% RH and 40 °C as feed conditions the amount of moles of H_2O fed is only 20% of the amount of moles of CO_2. Therefore, the aforementioned ratio is significantly lower and translates into an energy penalty of around 0.2 MJ/kg CO_2.

3.4.2. Results of Evaluation. The results of the analysis, shown in Figure 14, illustrate that the reaction heat is the major factor influencing the total energy needed for desorption. The reaction heat for the Lewatit sorbent (65 kJ/mol) is in the same range as for other amine sorbents.[26] Therefore, it might be difficult to reduce the contribution of the reaction heat in the total energy needed for desorption,

DOI: 10.1021/acs.iecr.8b00768
Ind. Eng. Chem. Res. 2018, 57, 11141−11153

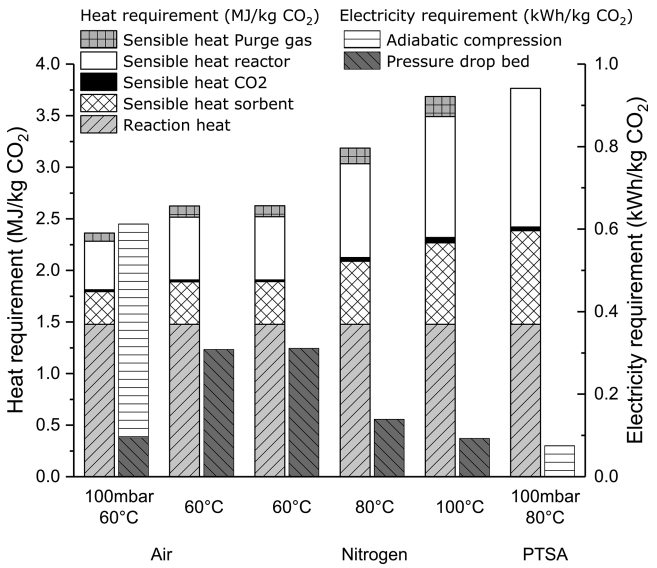

Figure 14. Required energy for the desorption with an adsorption velocity of 0.25 m/s.

although Fujiki et al.[27] reported a novel amine sorbent with reaction heat around 40 kJ/mol. Since the heat of reaction is the same for all regeneration options, the selection of the most attractive regeneration option will be independent of the absolute value of this reaction energy.

Furthermore, the sensible heats of the sorbent and the reactor are a significant factor in the total energy of desorption. The amount of sensible heat needed is mainly a function of working capacity and the desorption temperature. Increasing the working capacity and reducing the temperature will decrease the sensible heat needed. An increased working capacity will decrease sorbent mass and thereby reactor dimensions. This is shown for the 100 mbar and 60 °C air purge case in Figure 14 and Table 5. Nevertheless, for that case the reduction in sensible heat for the sorbent is penalized by the increase in the compression energy and thereby the advantage of the reduction in sensible heat is lost.

The sensible heat of the reactor can be minimized in a detailed design. For example, doubling the tube diameter will already halve the amount of steel needed, thereby reducing the sensible heat for the reactor. However, it should be ensured that heat transfer will not be negatively influenced, because the 30 min working capacity and hence the system productivity are strongly influenced by the experimental heating rate. In Section 3.3.3 it is shown that the productivity is a function of the equilibrium between the gas and the solid phase. As shown in Figure 1 the isotherm is a strong function of temperature. Therefore, it is expected that increasing the heating rate of the sorbent will increase the desorption rate significantly. Consequently, optimization of heat transfer and reaction dimensions will go hand in hand.

From Figure 14 it can be seen that in general the energy for the bed pressure drop is reducing with increasing working capacity. The major reason for this is that a lower amount of sorbent is needed with a higher working capacity. Less sorbent will result in a shorter column and therefore in a lower pressure drop. Next to increased sensible heat, more sorbent will lead to a longer column because the diameter of the reactor is held constant. Consequently, this will lead to a higher pressure drop. Moreover, for the presented design the purge flow will increase for the cases with lower working capacity to keep the CO_2/N_2 ratio equal to the experimental conditions. In this way, the concentration of CO_2 in the purge gas will be equal to experimental conditions of which the importance was shown in Section 3.3. Of course, in the final design the purge flow should be optimized for each temperature to make a more fair comparison. The exception to the trend is the PTSA case, where a relatively low working capacity also has a low compression energy, since only the produced CO_2 is compressed. On the other hand, the 100 mbar, 60 °C air purge case has a high energy demand for compression due to the large amount of gas flow that needs to be extracted to reduce the pressure.

Considering that the price of electric energy per MJ is significantly higher than that of thermal energy,[28] one might focus on the reduction of the electricity requirement in Table 5. Standing out is the PTSA case with low electricity need and medium heat requirements. Additionally, this is the only considered case that will deliver a high purity CO_2 gas product stream. On the other hand, a higher amount of sorbent is needed as a result of the lower working capacity. When one is not interested in the product gas and the evaluation is purely based on energy consumption, the 80 °C nitrogen purge is the case with the lowest energy consumption during desorption. It has a low electricity requirement and needs less sorbent due to increased working capacity. However, this is penalized by an increase in heat requirement. On the other hand, the air purge case at atmospheric pressure will have the advantage that the purge gas is significantly cheaper than nitrogen and therefore might be economically more favorable. However, due to increased sorbent mass the requirement of electricity (to overcome the pressure drop) is higher. It should be noted that it is expected that the electricity requirement can be reduced by optimizing the column design.

Purely based on the energy evaluation and a fixed reactor diameter, either the 80 °C PTSA or 80 °C nitrogen purge case

Table 5. Overview of Key Performance Indicators (KPI) and Column Dimensions for an Adsorption Velocity of 0.25 m/s

KPI	air, 60 °C, 100 mbar	air, 60 °C, 1 atm	N_2, 60 °C, 1 atm	N_2, 80 °C, 1 atm	N_2, 100 °C, 1 atm	PTSA 80 °C, 100 mbar
purge flow ($m_{purge}^3/m_{CO_2}^3$)	7.3	9.5	9.5	7.1	6.1	0
working capacity 30 min ($mol_{CO_2}\ kg_{sorbent}^{-1}$)	2.2	1.7	1.7	2.2	2.6	1.5
column length (m)	7.6	9.8	9.8	7.3	6.3	10.8
heat requirement (MJ $kg_{CO_2}^{-1}$)	2.4	2.6	2.6	3.2	3.7	3.8
electricity req (kW h $kg_{CO_2}^{-1}$)	0.6	0.3	0.3	0.1	0.1	0.1
desorption productivity ($mol_{CO_2}\ m_{reactor}^{-3}\ s^{-1}$)	0.7	0.5	0.5	0.7	0.8	0.5

DOI: 10.1021/acs.iecr.8b00768
Ind. Eng. Chem. Res. 2018, 57, 11141−11153

is the most promising case. As has been noted the PTSA case will deliver high purity CO_2 by a 8% penalty in heat requirement and a 50% increase in sorbent mass. However, when all economics of the process are taken into account and depending on local conditions with respect to prices or availability of "waste"-energy streams, one might come to other conclusions.

4. CONCLUSION

In this paper the regeneration conditions of a solid amine sorbent for the removal of CO_2 from biogas have been evaluated. Without purge flow, pressure swing adsorption is the most favorable option based on energy usage only. However, because of the very low working capacity, pressure swing adsorption alone is most likely not economic and should be combined with an increase in temperature (PTSA).

When a purge gas is used, it was found that the desorption rate is strongly influenced by the equilibrium between gas and solid phase. Because of the temperature dependency of the isotherm, heat transfer was determined to be a relevant parameter, also in relation to the rate of desorption. At lower temperatures even air can be used, albeit at the expense of lower working capacities and reduced desorption productivity. At higher temperatures (80 °C or higher) the working capacity increases drastically, but sensible heat requirements start to become significant. In the end, economics for purge gas costs, (local) costs for required heat and power, sorbent amount, and equipment size will need to be determined to be able to select the most optimal regeneration technology.

AUTHOR INFORMATION

Corresponding Author

*E-mail wim.brilman@utwente.nl. Phone: +31 53 489 2141.

ORCID

Martin J. Bos: 0000-0002-8049-8261

Notes

The authors declare no competing financial interest.

ACKNOWLEDGMENTS

The authors thank Institute for Sustainable Process Technology (ISPT) and the Dutch Ministry of Economic Affairs for financial support. Benno Knaken, Karst van Bree, and Johan Agterhorst are acknowledged for the construction of the experimental setup and their technical support during the experimental work.

REFERENCES

(1) Abatzoglou, N.; Boivin, S. A review of biogas purification processes. *Biofuels, Bioprod. Biorefin.* **2009**, *3*, 42−71.

(2) Andriani, D.; Wresta, A.; Atmaja, T. D.; Saepudin, A. A Review on Optimization Production and Upgrading Biogas Through CO2 Removal Using Various Techniques. *Appl. Biochem. Biotechnol.* **2014**, *172*, 1909−1928.

(3) Sonnleitner, E.; Schöny, G.; Hofbauer, H. Assessment of zeolite 13X and Lewatit® VP OC 1065 for application in a continuous temperature swing adsorption process for biogas upgrading. *Biomass Convers. Biorefin.* **2018**, *8*, 379.

(4) Sutanto, S.; Dijkstra, J. W.; Pieterse, J. A. Z.; Boon, J.; Hauwert, P.; Brilman, D. W. F. CO2 removal from biogas with supported amine sorbents: First technical evaluation based on experimental data. *Sep. Purif. Technol.* **2017**, *184*, 12−25.

(5) Veneman, R.; Frigka, N.; Zhao, W.; Li, Z.; Kersten, S.; Brilman, W. Adsorption of H2O and CO2 on supported amine sorbents. *Int. J. Greenhouse Gas Control* **2015**, *41*, 268−275.

(6) Alesi, W. R.; Gray, M.; Kitchin, J. R. CO2 adsorption on supported molecular amidine systems on activated carbon. *ChemSusChem* **2010**, *3*, 948−956.

(7) Drage, T. C.; Smith, K. M.; Arenillas, A.; Snape, C. E. Developing strategies for the regeneration of polyethylenimine based CO2 adsorbents. *Energy Procedia* **2009**, *1*, 875−880.

(8) Serna-Guerrero, R.; Belmabkhout, Y.; Sayari, A. Influence of regeneration conditions on the cyclic performance of amine-grafted mesoporous silica for CO2 capture: An experimental and statistical study. *Chem. Eng. Sci.* **2010**, *65*, 4166−4172.

(9) Drage, T. C.; Arenillas, A.; Smith, K. M.; Snape, C. E. Thermal stability of polyethylenimine based carbon dioxide adsorbents and its influence on selection of regeneration strategies. *Microporous Mesoporous Mater.* **2008**, *116*, 504−512.

(10) Pirngruber, G. D.; Leinekugel-le Cocq, D. Design of a Pressure Swing Adsorption Process for Postcombustion CO 2 Capture. *Ind. Eng. Chem. Res.* **2013**, *52*, 5985−5996.

(11) Aaron, D.; Tsouris, C. Separation of CO_2 from Flue Gas: A Review. *Sep. Sci. Technol.* **2005**, *40*, 321−348.

(12) Serna-Guerrero, R.; Belmabkhout, Y.; Sayari, A. Triamine-grafted pore-expanded mesoporous silica for CO2 capture: Effect of moisture and adsorbent regeneration strategies. *Adsorption* **2010**, *16*, 567−575.

(13) Schladt, M. J.; Filburn, T. P.; Helble, J. J. Supported amine sorbents under temperature swing absorption for CO 2 and moisture capture. *Ind. Eng. Chem. Res.* **2007**, *46*, 1590−1597.

(14) Lu, C.; Su, F.; Hsu, S. C.; Chen, W.; Bai, H.; Hwang, J. F.; Lee, H. H. Thermodynamics and regeneration of CO2 adsorption on mesoporous spherical-silica particles. *Fuel Process. Technol.* **2009**, *90*, 1543−1549.

(15) Veneman, R.; Hilbers, T.; Brilman, D. W. F.; Kersten, S. R. A. CO2 capture in a continuous gas-solid trickle flow reactor. *Chem. Eng. J.* **2016**, *289*, 191−202.

(16) Linstrom, P.; Mallard, W. In *NIST Chemistry WebBook, NIST Standard Reference Database Number 69*; Linstrom, P., Mallard, W., Eds.; National Institute of Standards and Technology: Gaithersburg, MD; DOI: 10.18434/T4D303.

(17) Jansen, L.; Warmoeskerken, M. *Transport phenomena data companion*, 3rd ed.; VSSD: Delft, 2006; p 159.

(18) Lanxess. *Lewatit VP OC 1065 Technical Data Sheet*; 2016.

(19) Green, D. W.; Perry, R. H. Pumps and Compressors. 1997; https://www.accessengineeringlibrary.com:443/browse/perrys-chemical-engineers-handbook-eighth-edition/p200139d899710_24001.

(20) Partington, J. R. The Ratio of the Specific Heats of Air and of Carbon Dioxide. *Proc. R. Soc. London, Ser. A* **1921**, *100*, 27−49.

(21) Bird, R. B.; Stewart, W. E.; Lightfoot, E. N. *Transport Phenomena*, 2nd ed.; John Wiley & Sons, Ltd.: 2007; p 928.

(22) Yu, Q.; Delgado, J. d. l. P.; Veneman, R.; Brilman, D. W. F. Stability of a Benzyl Amine Based CO2 Capture Adsorbent in View of Regeneration Strategies. *Ind. Eng. Chem. Res.* **2017**, *56*, 3259−3269.

(23) Veneman, R. Adsorptive systems for post-combustion CO2 capture: design, experimental validation and evaluation of a supported amine based process. Ph.D. thesis, University of Twente, Enschede, 2015.

(24) Ruthven, D. M. *Principles of Adsorption and Adsorption Processe*; John Wiley And Sons Ltd.: 1984; p 464.

(25) Seader, J. D.; Henley, E. J.; Roper, D. K. *Choice Reviews Online*, 3rd ed.; John Wiley And Sons Ltd.: 2010; p 848.

(26) Zhang, W.; Liu, H.; Sun, Y.; Cakstins, J.; Sun, C.; Snape, C. E. Parametric study on the regeneration heat requirement of an amine-based solid adsorbent process for post-combustion carbon capture. *Appl. Energy* **2016**, *168*, 394−405.

(27) Fujiki, J.; Chowdhury, F. A.; Yamada, H.; Yogo, K. *Chemical Engineering Journal*; Elsevier B.V.: 2017; Vol. *307*, pp 273−282, DOI: 10.1016/j.cej.2016.08.071.

DOI: 10.1021/acs.iecr.8b00768
Ind. Eng. Chem. Res. 2018, 57, 11141−11153

(28) Dutch Association of Cost Engineers. *Price booklet*, 30th ed.; BIM Media: The Hague, 2014.

DOI: 10.1021/acs.iecr.8b00768
Ind. Eng. Chem. Res. 2018, 57, 11141−11153